some loss of D^0 because of ionization is also possible. By using these results, we can extract the quantum process tomography (*25*) of the sequence, confirming the close resemblance to the identity operator.

The AEDMR mechanism we introduce here should be extensible to the readout of single ^{31}P impurities (*17*, *30*) and could be combined with the already demonstrated spin-dependent–tunneling electron spin readout of single ^{31}P (*14*). The method can be applied to other substitutional donors when ^{28}Si samples become available, and in particular Bi, where the much larger hyperfine coupling makes the hyperfine D^0X structure almost resolvable even in natural Si (*20*). The present p-type sample, together with our optical methods, would also be suited well to explore the NMR of ionized ^{31}P (D^+), which has recently been observed by using electrically detected ENDOR in natural Si (*13*) and should have very long T_{2n} in ^{28}Si. Such results would be important for the proposed cluster-state quantum computing scheme where quantum information is stored in the nuclear spins of ionized donors (*31*).

By eliminating almost all inhomogeneous broadening and host spins, highly enriched ^{28}Si approaches a semiconductor vacuum, enabling the use of hyperfine-resolved optical transitions, as is standard for atom and ion qubits in vacuum, but retaining the advantages of Si device technology, Auger photoionization for polarization and readout, and the ability to precisely and permanently place the qubit atoms (*32*).

References and Notes

1. D. Deutsch, *Proc. R. Soc. London Ser. A* **400**, 97 (1985).
2. J. P. Home *et al.*, *Science* **325**, 1227 (2009); 10.1126/science.1177077.
3. J. J. L. Morton, D. R. McCamey, M. A. Eriksson, S. A. Lyon, *Nature* **479**, 345 (2011).
4. P. Becker, H.-J. Pohl, H. Riemann, N. V. Abrosimov, *Phys. Status Solidi A* **207**, 49 (2010).
5. T. D. Ladd *et al.*, *Nature* **464**, 45 (2010).
6. B. E. Kane, *Nature* **393**, 133 (1998).
7. J. J. L. Morton *et al.*, *Nature* **455**, 1085 (2008).
8. D. R. McCamey, J. Van Tol, G. W. Morley, C. Boehme, *Science* **330**, 1652 (2010).
9. S. Simmons *et al.*, *Nature* **470**, 69 (2011).
10. A. M. Tyryshkin *et al.*, *Nat. Mater.* **11**, 143 (2012).
11. D. R. McCamey, J. van Tol, G. W. Morley, C. Boehme, *Phys. Rev. Lett.* **102**, 027601 (2009).
12. H. Morishita *et al.*, *Phys. Rev. B* **80**, 205206 (2009).
13. L. Dreher, F. Hoehne, M. Stutzmann, M. S. Brandt, *Phys. Rev. Lett.* **108**, 027602 (2012).
14. A. Morello *et al.*, *Nature* **467**, 687 (2010).
15. W. M. Witzel, M. S. Carroll, A. Morello, Ł. Cywiński, S. Das Sarma, *Phys. Rev. Lett.* **105**, 187602 (2010).
16. M. Cardona, M. L. W. Thewalt, *Rev. Mod. Phys.* **77**, 1173 (2005).
17. A. Yang *et al.*, *Phys. Rev. Lett.* **97**, 227401 (2006).
18. A. Yang *et al.*, *Phys. Rev. Lett.* **102**, 257401 (2009).
19. M. Steger *et al.*, *J. Appl. Phys.* **109**, 102411 (2011).
20. T. Sekiguchi *et al.*, *Phys. Rev. Lett.* **104**, 137402 (2010).
21. T. D. Ladd, D. Maryenko, Y. Yamamoto, E. Abe, K. M. Itoh, *Phys. Rev. B* **71**, 014401 (2005).
22. C. Langer *et al.*, *Phys. Rev. Lett.* **95**, 060502 (2005).
23. A. Yang *et al.*, *Appl. Phys. Lett.* **95**, 122113 (2009).
24. W. Schmid, *Phys. Status Solidi B* **84**, 529 (1977).
25. Materials and methods are available as supplementary materials on *Science* Online.
26. L. Viola, S. Lloyd, *Phys. Rev. A* **58**, 2733 (1998).
27. A. M. Tyryshkin *et al.*, http://arxiv.org/abs/:1011.1903v2 (2010).
28. T. Gullion, D. B. Baker, M. S. Conradi, *J. Magn. Reson.* **89**, 479 (1990).
29. G. Feher, E. A. Gere, *Phys. Rev.* **114**, 1245 (1959).
30. D. Sleiter *et al.*, *New J. Phys.* **12**, 093028 (2010).
31. J. J. L. Morton, http://arxiv.org/abs/0905.4008v1 (2009).
32. S. R. Schofield *et al.*, *Phys. Rev. Lett.* **91**, 136104 (2003).

Acknowledgments: This work was supported by the Natural Sciences and Engineering Research Council of Canada (NSERC). J.J.L.M. acknowledges support from the Royal Society (UK), St. John's College, Oxford, the Engineering and Physical Sciences Research Council (EP/I035536/1), and a European Research Council Starter Grant.

Supplementary Materials

www.sciencemag.org/cgi/content/full/336/6086/1280/DC1
Materials and Methods
Supplementary Text
Figs. S1 and S2
References (*33*–*37*)

8 December 2011; accepted 13 April 2012
10.1126/science.1217635

Room-Temperature Quantum Bit Memory Exceeding One Second

P. C. Maurer,[1]* G. Kucsko,[1]* C. Latta,[1] L. Jiang,[2] N. Y. Yao,[1] S. D. Bennett,[1] F. Pastawski,[3] D. Hunger,[3] N. Chisholm,[4] M. Markham,[5] D. J. Twitchen,[5] J. I. Cirac,[3] M. D. Lukin[1]†

Stable quantum bits, capable both of storing quantum information for macroscopic time scales and of integration inside small portable devices, are an essential building block for an array of potential applications. We demonstrate high-fidelity control of a solid-state qubit, which preserves its polarization for several minutes and features coherence lifetimes exceeding 1 second at room temperature. The qubit consists of a single ^{13}C nuclear spin in the vicinity of a nitrogen-vacancy color center within an isotopically purified diamond crystal. The long qubit memory time was achieved via a technique involving dissipative decoupling of the single nuclear spin from its local environment. The versatility, robustness, and potential scalability of this system may allow for new applications in quantum information science.

Many applications in quantum communication (*1*) and quantum computation (*2*) rely on the ability to maintain qubit coherence for extended periods of time. Furthermore, integrating such quantum-mechanical systems in compact mobile devices remains an outstanding experimental task. Although trapped ions and atoms (*3*) can exhibit coherence times as long as minutes, they typically require a complex infrastructure involving laser cooling and ultrahigh vacuum. Other systems, most notably ensembles of electronic and nuclear spins, have also achieved long coherence times in bulk electron spin resonance (ESR) and nuclear magnetic resonance (NMR) experiments (*4*–*6*); however, owing to their exceptional isolation, individual preparation, addressing, and high-fidelity measurement remain challenging, even at cryogenic temperatures (*7*).

Our approach is based on an individual nuclear spin in a room-temperature solid. A nearby electronic spin is used to initialize the nuclear spin (*8*–*10*) in a well-defined state and to read it out in a single shot (*10*) with high fidelity. A combination of laser illumination and radio-frequency (rf) decoupling pulse sequences (*4, 11*) enables the extension of our qubit memory lifetime by nearly three orders of magnitude. This approach decouples the nuclear qubit from both the nearby electronic spin and other nuclear spins, demonstrating that dissipative decoupling can be a robust and effective tool for protecting coherence in various quantum information systems (*2, 12, 13*).

Our experiments used an individual nitrogen-vacancy (NV) center and a single ^{13}C ($I = 1/2$) nuclear spin (Fig. 1A) in a diamond crystal. We worked with an isotopically pure diamond sample, grown using chemical vapor deposition from isotopically enriched carbon consisting of 99.99% spinless ^{12}C isotope. In such a sample, the optically detected ESR associated with a single NV center is only weakly perturbed by ^{13}C nuclear spins, resulting in long electronic spin coherence times (*14*). This allows us to make use of a Ramsey pulse sequence to detect a weakly coupled single nuclear spin, separated from the NV by 1 to 2 nm. The coupling strength at such a distance is sufficiently large to enable preparation and measurement of the nuclear-spin qubit with high fidelity. For the concentration of ^{13}C nuclei we used, about 10% of all NV centers exhibited a coupled nuclear spin with a separation of this order.

In our experimental setup, the diamond sample was magnetically shielded from external perturbations, and a static magnetic field $B = 244.42 \pm 0.02$ G was applied along the NV symmetry axis.

[1]Department of Physics, Harvard University, Cambridge, MA 02138, USA. [2]Institute for Quantum Information and Matter, California Institute of Technology, Pasadena, CA 91125, USA. [3]Max-Planck-Institut für Quantenoptik, Garching D-85748, Germany. [4]School of Engineering and Applied Sciences, Harvard University, Cambridge, MA 02138, USA. [5]Element Six, Ascot SL5 8BP, UK.

*These authors contributed equally to this work.
†To whom correspondence should be addressed. E-mail: lukin@physics.harvard.edu

The spin transition between the $|0\rangle \rightarrow |-1\rangle$ electronic spin states was addressed via microwave radiation (*15*). Figure 1B shows the free-electron precession of an individual NV center, measured via a Ramsey sequence. The signal dephased on a time scale of $T_{2e}^{*} = 470 \pm 100$ μs, which is consistent with the given isotopic purity of the sample (*14*). The characteristic collapses and revivals of the Ramsey signal correspond to the signature of a single weakly coupled ^{13}C nuclear spin. This coupling strength, originating from a hyperfine interaction, corresponds to an electron-nuclear separation of roughly 1.7 nm (*15*).

To confirm that the signal originated from a ^{13}C nuclear spin, we measured the probability of a rf-induced nuclear spin-flip as a function of carrier frequency, ω. As described below, we prepared the nuclear spin in either the $|\downarrow\rangle$ or $|\uparrow\rangle$ state by performing a projective measurement. After preparation of the nuclear spin via projection, a 1.25-ms Gaussian shaped rf π-pulse was applied. A second step of nuclear measurement then allowed the nuclear spin-flip to be determined. Figure 1C shows that this probability is characterized by three resonances located at $\omega/(2\pi) =$ 258.86, 261.52, and 264.18 kHz, corresponding to the NV electronic spin being in $m_s = 1,0,-1$, respectively; this indicates a projected hyperfine interaction $A_{\parallel} = (2\pi)\ (2.66 \pm 0.08)$ kHz.

An important facet of quantum control involves the ability to perform high-fidelity initialization and readout. We used repetitive readout to achieve single shot detection of the nuclear spin state. In this approach (Fig. 2A), the electronic spin is first polarized into the $|0\rangle$ state. Next, a C_nNOT_e logic gate (electronic spin-flip conditioned on the nuclear spin) is performed, and the resulting state of the electronic spin is optically detected; this sequence is repeated multiple times to improve the readout fidelity. The required quantum logic is achieved via a Ramsey sequence on the electronic spin, where the free precession time is chosen to be $\tau = \pi/A_{\parallel}$. Figure 2B depicts an example trace of the accumulated fluorescence of 20,000 readout repetitions per data point. The resulting signal clearly switches between two distinct values, which correspond to the two states of the spin-$\frac{1}{2}$ ^{13}C nuclear spin. We associate high count rates with the $|\uparrow\rangle$ state of the nuclear spin and low count rates with the $|\downarrow\rangle$ state, noting that these do not necessarily correspond to alignment/anti-alignment with the external field (*15*). This time trace indicates that the nuclear spin preserves its orientation, on average, for about half a minute.

To achieve high-fidelity initialization of the nuclear spin, we post-selected repetitive readout measurements that were below a threshold corresponding to 147 counts per 2.2 s and above a threshold corresponding to 195 counts per 2.2 s. This allowed us to prepare the nuclear spin state with >97% fidelity (*15*). After successful initialization via projection, a second repetitive readout measurement was performed. This allowed us to extract readout count statistics dependent on the nuclear spin state. As shown in Fig. 2C, the two distributions for the count rates of $|\uparrow\rangle$ and $|\downarrow\rangle$ are clearly resolved, and their medians match the high and low levels of the fluorescence trace in Fig. 2B. From the overlap between the two distributions, we obtain a projective readout fidelity of 91.9 ± 2.5% (*16*).

The long spin-orientation lifetime, extracted from Fig. 2B, implies that our ^{13}C nuclear spin is an exceptionally robust degree of freedom. To quantify the nuclear depolarization rate, the T_{1n} time was measured as a function of laser intensity. In the dark, no decay was observed on a time scale of 200 s (*15*). However, consistent with predictions from a spin-fluctuator model (*17, 18*), when illuminated with a weak optical field, T_{1n} dropped to 1.7 ± 0.5 s and increased linearly for higher laser intensities (Fig. 2D).

To probe the qubit's coherence time, our nuclear spin was again prepared via a projective measurement, after which an NMR Ramsey pulse sequence was applied. The final state of the nuclear spin was then detected via repetitive readout. The results (Fig. 3B) demonstrate that, in the dark, the nuclear coherence time T_{2n}^{*} is limited to about 8.2 ± 1.3 ms. The origin of this relatively fast dephasing time can be understood by noting its direct correspondence with the population lifetime of the electronic spin $T_{1e} = 7.5 \pm 0.8$ ms (blue curve in Fig. 3B) (*19*). Because the electron-nuclear coupling $A_{\parallel}$ exceeds $1/T_{1e}$, a single (random) flip of the electronic spin (from $|0\rangle$ to $|\pm1\rangle$) is sufficient to dephase the nuclear spin.

To extend the nuclear memory time, we must effectively decouple the electronic and nuclear spin during the storage interval. This is achieved by subjecting the electronic spin to controlled dissipation. Specifically, the NV center is excited by a focused green laser beam, resulting in optical pumping of the NV center out of the magnetic states ($|\pm1\rangle$). In addition, the NV center also undergoes rapid ionization and deionization at a rate γ, proportional to the laser intensity (Fig. 3A). When these transition rates exceed the hyperfine coupling strength, the interaction between the nuclear and electronic spins is strongly suppressed, owing to a phenomenon analogous to motional averaging (*17*).

Using this decoupling scheme, we show in Fig. 3C that the nuclear coherence time can be

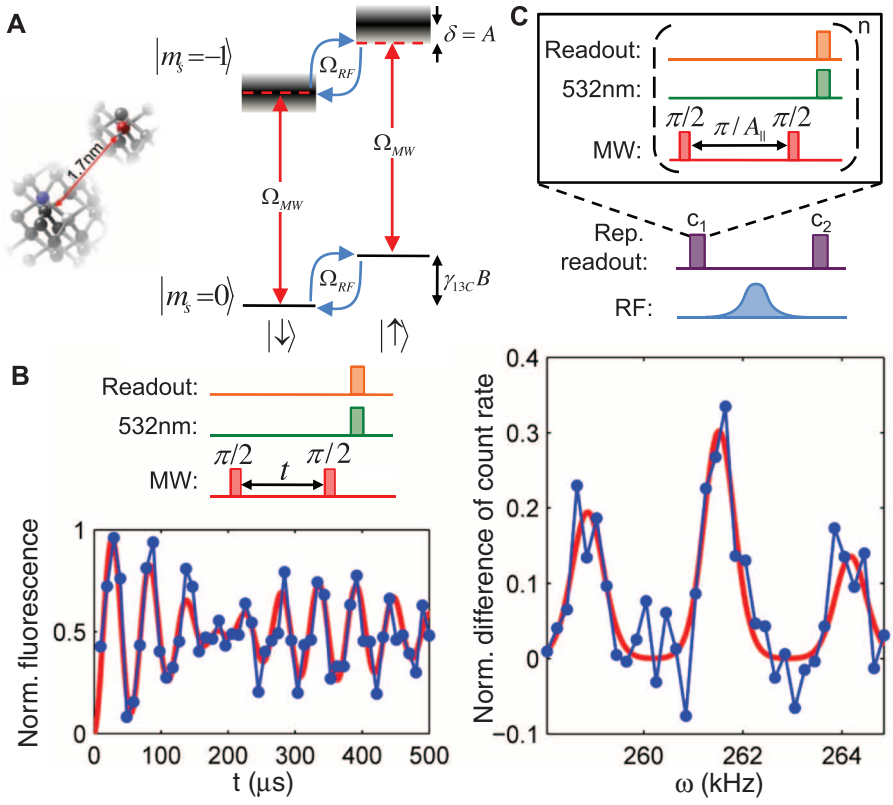

Fig. 1. Experimental system. (**A**) The NV center with a proximal ^{13}C spin can be modeled as a simple four-level system to understand readout dynamics. Nuclear spin sublevels $|\uparrow\rangle$ and $|\downarrow\rangle$ are split by a Zeeman shift ($\gamma_{^{13}C}B$) and addressed via rf radiation with Rabi frequency Ω_{RF}. The electronic transition $|0\rangle \rightarrow |-1\rangle$ (red arrows) can be simultaneously driven by a microwave (MW) field with relative detuning given by the hyperfine coupling strength $A_{\parallel}$. (**B**) An electron Ramsey measurement (blue points) as a function of free evolution time (t) depicts beating due to the different hyperfine transitions and a fitted $T_{2e}^{*} = 470 \pm 100$ μs (red solid line). (**C**) NMR spectra of ^{13}C, obtained via the depicted pulse sequence, demonstrate three different nuclear transitions corresponding to electronic spin states $m_s = 0,\pm1$. The pulse sequence contains a (blue) Gaussian rf pulse and two repetitive readouts (purple), c_1 and c_2.

enhanced by simply applying green laser light; in particular, 10 mW of green laser excitation yield an extended nuclear coherence time of $T_{2n}^{*} = 0.53 \pm 0.14$ s. This is an improvement of T_{2n}^{*} by almost two orders of magnitude as compared with measurements in the dark. The dependence of T_{2n}^{*} on green laser intensity shows a linear increase for low intensities and saturates around 1 s (Fig. 3E).

The observed limitation of coherence enhancement arises from dipole-dipole interactions of the nuclear qubit with other ^{13}C nuclei in the environment. In our sample, we estimate this average dipole-dipole interaction to be ~1 Hz, consistent with the limit in the observed coherence time. Further improvement of the nuclear coherence is achieved via a homonuclear rf decoupling sequence. The composite sequence (Fig. 3D) is designed to both average out the internuclear dipole-dipole interactions (to first order) and to compensate for magnetic field drifts. Applying this decoupling sequence in combination with green excitation can further extend the coherence time to beyond 1 s (Fig. 3E, blue points).

These measurements demonstrate that individual nuclear spins in isotopically pure diamond are exceptional candidates for long-lived memory qubits. The qubit memory performance was fully quantified by two additional measurements. First, the average fidelity was determined by preparing and measuring the qubit along three orthogonal directions. The average fidelity, $\overline{F} = 1/2(1 + \langle C \rangle)$, was extracted from the observed contrast (C) of the signal and is presented in Fig. 4A for two cases (with and without homonuclear decoupling) (*8*). Even for memory times up to 2.11 ± 0.3 s, the fidelity remained above the classical limit of $\frac{2}{3}$. Finally, a full characterization of our memory (at 1 s of storage time) was obtained via quantum process tomography. The corresponding χ matrix (Fig. 4C) reveals an average fidelity, $\overline{F} = 87 \pm 5\%$ (*15*).

To quantitatively understand the coherence extension under green illumination, we consider depolarization and dephasing of the nuclear spin due to optical illumination and interaction with the nuclear spin environment. Excitation with 532 nm ionizes, as well as deionizes, the NV center with a rate proportional to the laser intensity (*20*). Adding up the peak probabilities (Fig. 1C) for the nuclear rf transitions reveals a total transition probability of 63 ± 5%. This is consistent with recent observations in which, under strong green illumination, the NV center is found to spend 30% of its time in an ionized state (*20*). In this state, rf-induced nuclear transitions are suppressed, because the depolarization rate of the electronic spin is much faster than the nuclear Rabi frequency (*20*). Because the hyperfine interaction is much smaller than the electronic Zeemann splitting, flip-flop interactions between the electronic and nuclear spins can be neglected. However, in the presence of an off-axis dipolar hyperfine field $A_{\perp}$, nuclear depolarization still occurs at a rate $1/T_{1n} \sim \frac{A_{\perp}^2}{(\gamma_{^{13}C}B/2)^2 + \gamma^2}\gamma$ (*15*). Although this simple analysis is already in good agreement with our observations (Fig. 2D), further insight is provided by a detailed 11-level model of NV dynamics (*15*). Because T_{1n} limits our readout, a careful alignment of the external field (i.e., choosing $A_{\perp} \to 0$) and enhanced collection efficiency should enable readout fidelities greater than 99%.

For ionization rates γ much larger than the hyperfine interaction, the dephasing rate depends on the parallel component of the dipole field, $1/T_{2n}^{*} = \Gamma_{opt} + \Gamma_{dd}$, where Γ_{dd} is the spin-bath–induced dephasing rate and $\Gamma_{opt} \sim \frac{A_{\parallel}^2}{\gamma}$ is the optically induced decoherence. The dashed red line in Fig. 3E demonstrates that this model is in good agreement with our data. Application of our decoupling sequence also allows us to suppress nuclear-nuclear dephasing. We find that the main imperfection in this decoupling procedure originates from a finite rf detuning (*15*). Accounting for this imperfection, we find excellent agreement with our data, as shown by the dashed blue line in Fig. 3E. Moreover, this model indicates that the coherence time increases almost linearly as a function of applied laser intensity, suggesting a large potential for improvement.

The use of even higher laser intensities is limited by heating of the diamond sample, which causes drifts in the ESR transition (*21*). However, this can be overcome via a combination of temperature control and careful transition-frequency tracking, yielding an order of magnitude improvement in the coherence time to approximately 1 min. Further improvement can be achieved by decreasing the hyperfine and nuclear-nuclear interaction strengths through a reduction of the ^{13}C concentration, potentially resulting in hour-long storage times (*15*). Finally, it is possible to use coherent decoupling sequences and techniques based on optimal control theory (*22*), which scale more favorably than our current dissipation-based method. With such techniques, we estimate that the memory lifetime can approach the time scale of phonon-induced nuclear depolarization, measured to exceed $T_{1n}^{max} \sim 36$ hours (*23*).

As a future application of our techniques, the realization of fraud-resistant quantum tokens can be considered. Here, secure bits of information are encoded into long-lived quantum memories. Along with a classical serial number, an array of such memories may possibly constitute a unique unforgeable token (*24, 25*). With a further enhancement of storage times, such tokens may potentially be used as quantum-protected credit cards or quantum identification cards (*25*), with absolute security. Furthermore, NV-based quantum registers can take advantage of the nuclear spin for storage, while using the electronic spin for quantum gates and readout (*8, 9*). In particular,

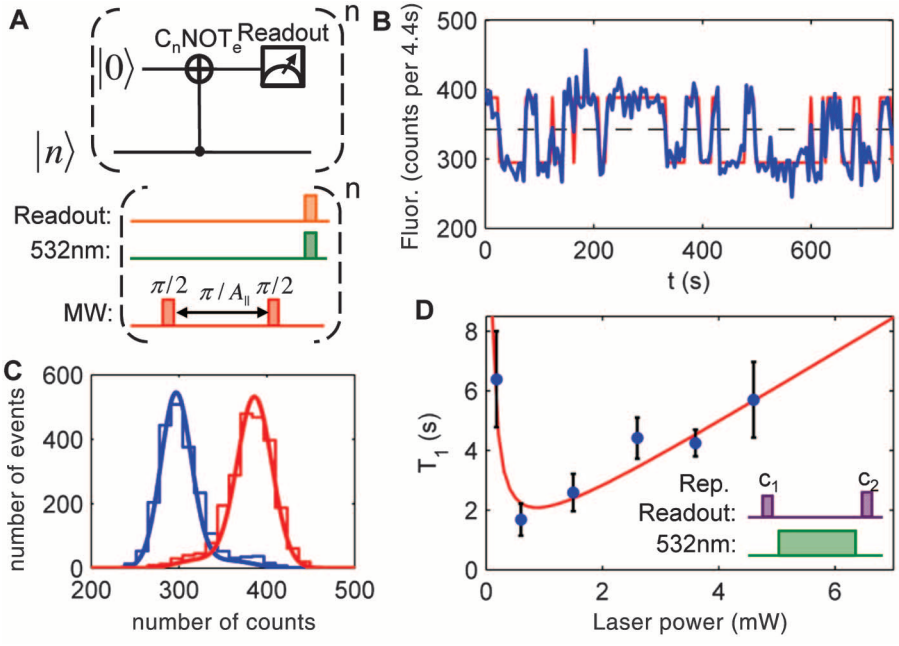

Fig. 2. Qubit readout. (**A**) Circuit diagram of repetitive readout of the nuclear spin $|n\rangle$. The readout uses multiple C_nNOT_e gates consisting of an electronic spin Ramsey followed by readout and repolarization. (**B**) Fluorescence time trace (blue data, red fit) showing single-shot readout of the nuclear spin and corresponding quantum jumps. The integration time for a single point is 4.4 s. (**C**) Histogram of continuous repetitive readouts (per 4.4 s) showing two overlapping distributions of nuclear spin states: $|\downarrow\rangle$ (blue) and $|\uparrow\rangle$ (red) (*15*). (**D**) Nuclear spin orientation lifetime, T_{1n} (here and below error bars are 1 SD) as a function of laser power in the presence of illumination by a 532-nm laser. As shown in the inset (bottom right), each data point is extracted from a series of two repetitive readout sequences. The solid red curve represents the theoretical prediction from the simple model of nuclear depolarization induced by the off-axis dipolar hyperfine field.

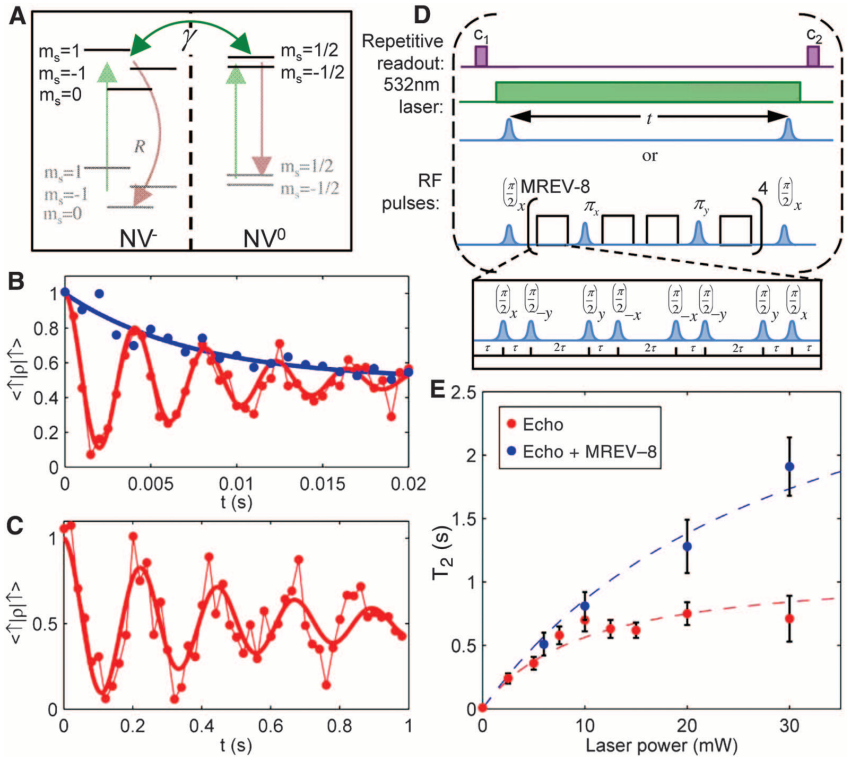

Fig. 3. Nuclear spin coherence. (**A**) Model for repolarization and ionization dynamics. In the NV^- charge state, the electronic spin can be pumped via green illumination to $m_s = 0$ at a rate R. (**B**) Nuclear Ramsey experiment (red curve) depicting a dephasing time $T_{2n}^* = 8.2 \pm 1.3$ ms. The origin of this dephasing is the depolarization of the electronic spin (blue curve), with $T_{1e} = 7.5 \pm 0.8$ ms. (**C**) Nuclear Ramsey experiment with concurrent green illumination, showing $T_{2n}^* = 0.53 \pm 0.14$ s. (**D**) Experimental sequence used to measure the nuclear coherence time. A modified Mansfield-Rhim-Elleman-Vaughan (MREV) decoupling sequence (*4*) is used. It consists of 16 MREV-8 pulse trains interwoven with eight phase-refocusing π-pulses. Each MREV-8 pulse sequence can be achieved through $\pi/2$ rotations around four different axes. (**E**) Nuclear coherence as a function of green laser power. The red data constitute a measurement of T_{2n} using a nuclear spin echo; blue data T_{2n} contain the additional MREV sequence. The dashed fits are calculated from the spin-fluctuator model (*15*). Each data point is extracted via a measurement analogous to that in (C).

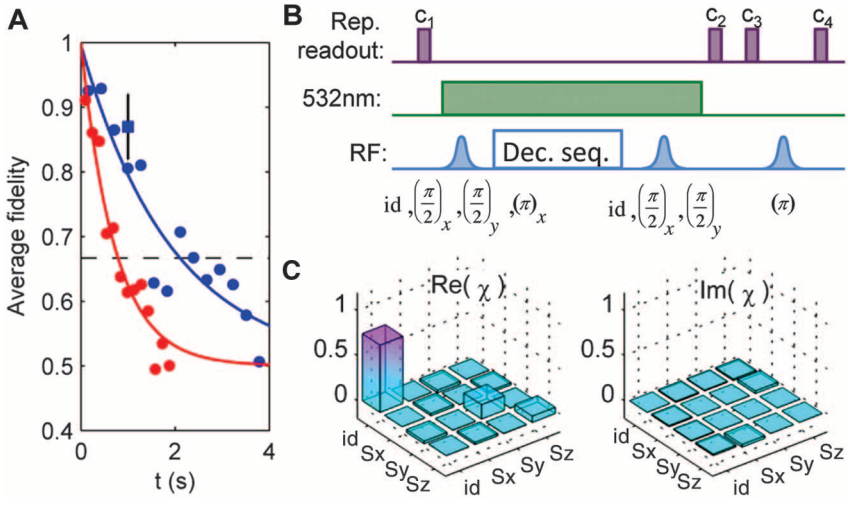

Fig. 4. Nuclear memory fidelity. (**A**) Average fidelity as a function of time obtained from states prepared along $|x\rangle = \frac{1}{\sqrt{2}}(|\downarrow\rangle + |\uparrow\rangle)$, $|y\rangle = \frac{1}{\sqrt{2}}(|\downarrow\rangle + i|\uparrow\rangle)$, and $|z\rangle = |\downarrow\rangle$. The nuclear echo (red curve) is obtained at 10 mW of green power, whereas the MREV sequence (blue curve) is obtained at 30 mW of green power. The square data point represents the fidelity extracted from process tomography. (**B**) Pulse sequence depicting the initialization of four different nuclear states and three subsequent rotations. (**C**) The χ matrix of the full quantum process tomography at 1 s of storage time with 30 mW of continuous green illumination (*15*).

recent progress in the deterministic creation of arrays of NV centers (*26*) and NV-C pairs (*27*) enables the exploration of scalable architectures (*28, 29*). Finally, recent experiments have also demonstrated the entanglement of a photon with the electronic spin state of an NV center (*30*). Combining the advantages of an ultralong nuclear quantum memory with the possibility of photonic entanglement opens up new routes to long-distance quantum communication and solid-state quantum repeaters (*1*).

References and Notes

1. L. M. Duan, C. Monroe, *Rev. Mod. Phys.* **82**, 1209 (2010).
2. T. D. Ladd *et al.*, *Nature* **464**, 45 (2010).
3. C. Langer *et al.*, *Phys. Rev. Lett.* **95**, 060502 (2005).
4. T. D. Ladd, D. Maryenko, Y. Yamamoto, E. Abe, K. Itoh, *Phys. Rev. B* **71**, 014401 (2005).
5. M. V. Balabas, T. Karaulanov, M. P. Ledbetter, D. Budker, *Phys. Rev. Lett.* **105**, 070801 (2010).
6. A. M. Tyryshkin *et al.*, *Nat. Mater.* **11**, 143 (2011).
7. A. Morello *et al.*, *Nature* **467**, 687 (2010).
8. M. V. Gurudev Dutt *et al.*, *Science* **316**, 1312 (2007).
9. T. van der Sar *et al.*, http://arxiv.org/abs/arXiv:1202.4379v1 (2012).
10. P. Neumann *et al.*, *Science* **329**, 542 (2010).
11. G. de Lange, Z. H. Wang, D. Ristè, V. V. Dobrovitski, R. Hanson, *Science* **330**, 60 (2010).
12. J. T. Barreiro *et al.*, *Nature* **470**, 486 (2011).
13. H. Krauter *et al.*, *Phys. Rev. Lett.* **107**, 080503 (2011).
14. G. Balasubramanian *et al.*, *Nat. Mater.* **8**, 383 (2009).
15. Materials and methods are available as supplementary materials on *Science* Online.
16. A. H. Burrell, D. J. Szwer, S. C. Webster, D. M. Lucas, *Phys. Rev. A* **81**, 040302 (2010).
17. L. Jiang *et al.*, *Phys. Rev. Lett.* **100**, 073001 (2008).
18. L. Jiang *et al.*, *Science* **326**, 267 (2009).
19. P. Neumann *et al.*, *Science* **320**, 1326 (2008).
20. G. Waldherr *et al.*, *Phys. Rev. Lett.* **106**, 157601 (2011).
21. V. M. Acosta *et al.*, *Phys. Rev. Lett.* **104**, 070801 (2010).
22. N. Khaneja, R. Brockett, R. J. Glaser, *Phys. Rev. A* **63**, 032308 (2001).
23. C. J. Terblanche, E. C. Reynhardt, J. A. van Wyk, *Solid State Nucl. Magn. Reson.* **20**, 1 (2001).
24. S. Wiesner, *ACM SIGACT News* **15**, 78 (1983).
25. F. Pastawski, N. Y. Yao, L. Jiang, M. D. Lukin, J. I. Cirac, http://arxiv.org/abs/1112.5456v1 (2011).
26. D. M. Toyli, C. D. Weis, G. D. Fuchs, T. Schenkel, D. D. Awschalom, *Nano Lett.* **10**, 3168 (2010).
27. P. Spinicelli *et al.*, *New J. Phys.* **13**, 025014 (2011).
28. N. Y. Yao *et al.*, *Nat. Commun.* **3**, 800 (2012).
29. P. Neumann *et al.*, *Nat. Phys.* **6**, 249 (2010).
30. E. Togan *et al.*, *Nature* **466**, 730 (2010).

Acknowledgments: We thank F. Jelezko, P. Neumann, J. Wrachtrup, R. Walsworth, A. Zibrov, and P. Hemmer for stimulating discussions and experimental help. This work was supported in part by NSF, the Center for Ultracold Atoms, the Defense Advanced Research Projects Agency (QUEST and QUASAR programs), Air Force Office of Scientific Research (MURI program), Element 6, the Packard Foundation, the European Union (DIAMANT program), a Fulbright Science and Technology Award (P.C.M.), the Swiss National Science Foundation (C.L.), the Sherman Fairchild Foundation, and the National Basic Research Program of China (973 program), grant 2011CBA00300 (2011CBA00301) (L.J.), the Department of Energy (FG02-97ER25308) (Y.Y.N).

Supplementary Materials

www.sciencemag.org/cgi/content/full/336/6086/1283/DC1
Materials and Methods
Supplementary Text
Figs. S1 to S12
References (*31–44*)

14 February 2012; accepted 17 April 2012
10.1126/science.1220513

Science

Room-Temperature Quantum Bit Memory Exceeding One Second

P. C. Maurer, G. Kucsko, C. Latta, L. Jiang, N. Y. Yao, S. D. Bennett, F. Pastawski, D. Hunger, N. Chisholm, M. Markham, D. J. Twitchen, J. I. Cirac and M. D. Lukin

Science **336** (6086), 1283-1286.
DOI: 10.1126/science.1220513

Extending Quantum Memory

Practical applications in quantum communication and quantum computation require the building blocks—quantum bits and quantum memory —to be sufficiently robust and long-lived to allow for manipulation and storage (see the Perspective by **Boehme and McCarney**). **Steger *et al.*** (p. 1280) demonstrate that the nuclear spins of ^{31}P impurities in an almost isotopically pure sample of ^{28}Si can have a coherence time of as long as 192 seconds at a temperature of ~ 1.7 K. In diamond at room temperature, **Maurer *et al.*** (p. 1283) show that a spin-based qubit system comprised of an isotopic impurity (^{13}C) in the vicinity of a color defect (a nitrogen-vacancy center) could be manipulated to have a coherence time exceeding one second. Such lifetimes promise to make spin-based architectures feasible building blocks for quantum information science.